Biol. Cybern. 78, 399–412 (1998)

Biological Cybernetics

Neural network model of on-off units in the fly visual system: simulations of dynamic behavior

Mert Sarikaya, Wenxia Wang, Haluk Öğmen

Department of Electrical and Computer Engineering, University of Houston, Houston, TX 77204-4793, USA

Received: 26 May 1997 / Accepted in revised form: 19 February 1998

Abstract. We analyze the dynamic properties of a neural network model for on-off spiking neurons recorded in the first optic chiasm of the fly visual system. The model consists of two parallel pathways and three sequential processing stages. The first stage models photoreceptors. At the second stage, the signal is segregated into on- and off-pathways. These pathways are proposed to correspond to two populations of amacrine cells. At the third stage, the on- and off-pathways converge to on-off neurons. Furthermore, according to the model, on-off neurons interact via recurrent connections. This stage is proposed to correspond to lamina L4 neurons. In response to luminance increments and decrements, the model exhibits a three-component response and suggests pathways for each of the components. When stimulated by a train of pulses, the model exhibits fast adaptation for frequencies higher than about 5 Hz. Furthermore, adaptation to on- and off-pulses occurs independently. When the frequency of stimulation is reduced, the unit recovers rapidly from its adapted state. The temporal modulation transfer function has its peak around 7 Hz. The phase characteristics show a phase lead for low temporal frequencies changing to a phase lag for high frequencies. These model predictions are compared with data from Jansonius and van Hateren (1991).

1 Introduction

The visual ganglia of the fly nervous system possess a highly organized columnar structure. Each column, or cartridge, in the first ganglion, the lamina, contains several cell types forming parallel channels for the visual system (review: Laughlin 1984; Shaw 1984). Three monopolar cells, L1, L2, and L3, which are directly postsynaptic to photoreceptors produce output signals in the form of transient hyperpolarizing graded-potentials to light stimulus. A fourth output comes from the basket cell T1. While little is known about this cell, it has been suggested that it produces graded hyperpolarizations like the second-order monopolar cells L1–L3 (see Shaw 1981; James and Osorio 1996). The other outputs of the lamina cartridge come from the third-order monopolar cells L4 and L5. These neurons receive their inputs from amacrine cells which are directly postsynaptic to photoreceptors. The present knowledge regarding the amacrine cells consists mainly of their anatomical characteristics. While the large monopolar cells L1 and L2 have been extensively studied (Laughlin 1984), electrophysiological studies of L4 and L5 have been limited. Until recently, the main findings about these cells were the electrophysiological recordings reported by Arnett (1972).[1]

A better understanding of these cells is important for at least two reasons: First, L4 and L5 provide qualitatively distinct output channels from the lamina cartridges (sustained versus transient; spike coding with half- and full-wave rectification versus graded-potential coding with sign conservation). Therefore, a complete picture of early visual processing in the fly nervous system necessitates an understanding of these cells. Second, due to the aforementioned unique properties of L4 and L5, these neurons have been proposed to constitute the front-end of the motion detection circuit (e.g. Öğmen and Gagné, 1990a). As a result, a better understanding of L4 and L5 may be instrumental in distinguishing among various types of models proposed for the motion processing circuit of flies (see, for example, Coombe et al. 1989; Egelhaaf and Borst 1992), thereby achieving a better understanding of the neural correlates of motion detection.

In our earlier work, we proposed neural network models for these sustained and transient units (Öğmen and Gagné 1990a). While the model for the sustained unit has been tested with the various experimental par-

Correspondence to: H. Öğmen
(e-mail: ogmen@uh.edu, Fax: +1-713-743-4444)

[1] Although Arnett could not directly identify his recordings with L4 and L5, various lines of evidence suggest that the cells he recorded from were L4 and L5 (Shaw 1981; Laughlin 1984).

adigms utilized by Arnett (1972), testing of the transient model has been limited due to a lack of experimental findings. Recently, Jansonius and van Hateren (1991, 1993a,b) reported extensive electrophysiological studies that replicated and extended the earlier findings of Arnett on L4 and L5 units. In this paper, we present a more detailed version of the on-off unit model and compare its temporal behavior with Jansonius and van Hateren's data. In order to compare the model directly with data, our simulations follow the general paradigms used by Jansonius and van Hateren.

2 Description of the model

2.1 Fundamental equations of the model

Two types of equations are used in the model. The first one describes the membrane potential of neurons and has the form of a generic Hodgkin–Huxley type model:

$$\frac{dV_{\mathrm{m}}}{dt} = (V^{\mathrm{p}} - V_{\mathrm{m}})g^{\mathrm{p}} + (V^{+} - V_{\mathrm{m}})g^{+} - (V^{-} + V_{\mathrm{m}})g^{-} \quad (1)$$

where V_{m} represents the membrane potential, g^{p} is the lumped conductance for passive channels. g^{+} represents a lumped conductance for gated channels such that an increase in conductance causes a depolarization in the membrane potential, for example, sodium channels, which involve a positively charged ion with a higher concentration on the outside of the cell. g^{-} represents a lumped conductance for gated channels such that an increase in conductance causes a hyperpolarization in the membrane potential, for example, potassium channels, which involve a positively charged ion with a higher concentration on the inside of the cell. V^{p}, V^{+}, V^{-} represent the reversal, or Nernst, potentials for these channels. Note that this equation is lumped in that it models a complete neuron rather than a small patch of membrane.

The second equation is used to describe synaptic transmission. In general, chemical synaptic transmission is a complex process. Little is known about the specifics of synaptic transmission leading to the L4 neurons in the fly lamina (type of transmitter, receptor, etc.). Therefore, we do not intend to model synaptic transmission processes in detail. However, we propose a process of short-term depression in synaptic efficiency (rev. Magleby 1987) as a correlate for fast temporal-adaptation effects. As we show now, a simple first-order biochemical equation can give an approximation for such a process. In general terms, let S represent a substance whose concentration depends on the presynaptic signal, and let Z represent an intermediate agent. Assume that S and Z combine to produce an 'active complex' Y which decays to an inactive state X. Finally, assume that the postsynaptic potential is proportional to the concentration of the 'active complex' Y. A first-order scheme for this process can be written as:

$$S + Z \xrightarrow{\gamma} Y \xrightarrow{\delta} X \xrightarrow{\alpha} S + Z \quad (2)$$

where γ, δ, and α denote rates of complex formation, decay to inactive state, and dissociation, respectively. If we denote by $s(t)$, $z(t)$, $y(t)$, and $x(t)$ the concentrations of S, Z, Y, and X respectively, and if we assume that the active state decays very fast (i.e. $\delta \gg \alpha, \gamma$), then the following equations can describe the dynamics of the system (see Appendix for details):

$$\frac{dz(t)}{dt} \approx \alpha(\beta - z) - \gamma s z \quad (3)$$

and

$$y(t) \approx (\gamma/\delta)s(t)z(t) \quad (4)$$

The postsynaptic potential is proportional to $y(t)$ and therefore to the product of $s(t)$ and $z(t)$. Solving (3) for a step input (i.e., $s(t) = u(t)$, where $u(t)$ is the unit-step function) one finds for $t > 0$:

$$z(t) = \frac{\beta}{\alpha + \gamma}(\alpha + \gamma \mathrm{e}^{-(\alpha+\gamma)t}) \quad (5)$$

which is a strictly decreasing function of time. As a result, for a constant input, the 'gain of the synapse' is decreased via $z(t)$, thereby generating a short-term depression in synaptic efficiency.

Although the actual process is much more complicated, the simple model given above captures the basics of synaptic depression, namely the decrease of synaptic efficiency for a sustained signal. This equation enjoys various physiological interpretations depending on how the modeled variables are mapped to the elements in the biochemical chain: A simple interpretation is to have $z(t)$ represent the amount of available transmitter and β the maximum amount of storable transmitter. As a result, the first and second terms on the right-hand side of (3) correspond to replenishment and depletion of transmitter, respectively. Another interpretation is to have $s(t)$ represent the amount of released transmitter and $z(t)$ the amount of available receptor sites.

When there is no short-term depression at a particular synapse, we model it by a static gain. Otherwise, we use (3) and (4).

Both of these basic equations [(1) and (3)–(4)] have been used in several neural models (e.g., Carpenter and Grossberg 1981; Grossberg 1982, 1988). In particular, the use of (3) and (4) in an opponent circuit leads to a neural module called the 'gated dipole' (Grossberg 1972), which forms the basis of our original model for on-off neurons.

2.2 The on-off model

Figure 1 shows the original model, called the 'augmented gated dipole' for transient on-off units (Öğmen and Gagné 1990a). The model has two parallel channels, one receiving the external input J_{i} and a baseline signal I, called the on-channel, and the second receiving only the baseline signal I, called the off-channel. The baseline signal is introduced to account for residual activity in the dark-adapted state. In all figures, the rectangular and

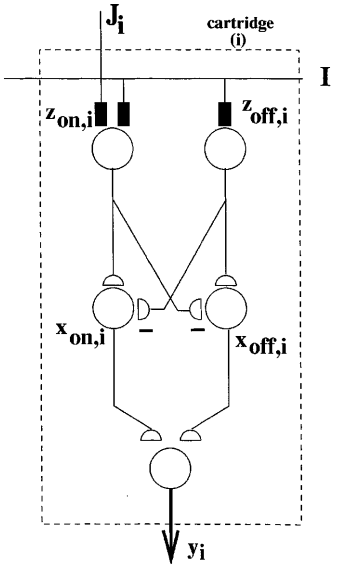

Fig. 1. The original version of the model for on-off units (Öğmen and Gagné 1990b). This version assumes that the receptive field is spatially homogeneous and therefore lumps all inputs into a single one, denoted by J_i. I represents a baseline signal introduced to account for residual activity in the dark-adapted state. The square and circular 'synapses' depict dynamic and static approximation, respectively. The variable z describes the dynamics of short-term adaptation. After the first stage of processing, corresponding to photoreceptors, the input is split into on- and off-channels, whose activities are described by x_{on} and x_{off}, respectively. These pathways then converge at a third-order neuron that models the on-off units. The activity of this cell is represented by y_i

half-circular 'synapses' depict synapses that are modeled with dynamic equations and static approximations, respectively.

At the second stage, these two channels inhibit each other, as shown by the lateral connections in Fig. 1. Finally, at a third stage, the outputs of the on- and off-channels converge with excitatory connections to a cell which models the on-off unit. The simulations reported in Öğmen and Gagné (1990a) consisted of responses to luminance increments and decrements of varying amplitudes. Arnett described the spatial aspect of the receptive fields of these units as 'homogeneous', i.e., the same type of output was generated from all parts of the receptive field (Arnett 1972). As a result, the original model comprised a single input representing the entire extent of the receptive field. More recent data, however, indicate that lateral inhibition exists in the receptive field of these units (Jansonius and van Hateren 1993a). The experimental paradigm consisted of stimulating the on-off unit by two light-emitting diodes (LEDs) placed symmetrically around the center of the receptive field, approximately 5 deg apart from each other (Jansonius and van Hateren 1993a). The luminance values of the LEDs either stayed at a baseline level or were incremented/decremented. Overall, the results showed that the luminance increment or decrement of one LED alone generates approximately the same response. A simultaneous luminance increment of both LEDs generates a weaker response. A decrement of the luminance of one LED while the luminance of the other is incremented produces a stronger response than a single increment. These observations suggest inhibitory interactions within the receptive field. To incorporate this finding into the model, we introduce lateral connections at two levels as shown in Fig. 2: The first consists of inhibitory connections among neighboring on-cells, and the second of excitatory recurrent connections among the on-off cells. Finally, unlike the

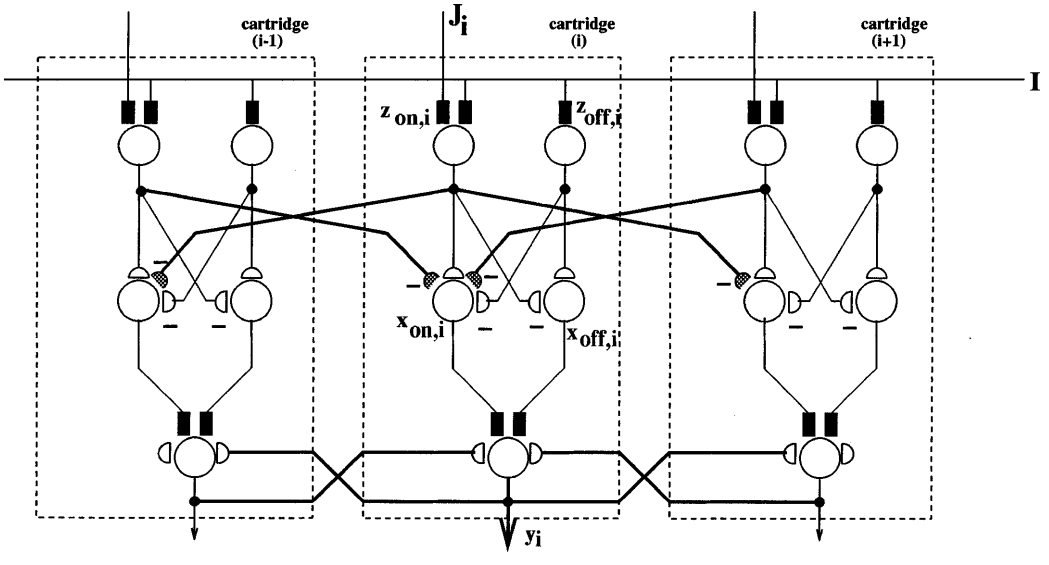

Fig. 2. The modified model for on-off units, incorporating lateral interactions within the receptive field. Each cartridge contains a copy of the original model. Bold lines between cartridges depict the lateral connections introduced to model interactions within the receptive field. The first level of lateral connections is between the on-cells. They correspond to dendritic interactions among putative on-amacrine cells. The second level of lateral connections occurs as feedback between third-order (on-off) cells. They correspond to anatomically identified connections between L4 cells. As in the previous figure, the square- and semicircular-shaped connections depict dynamic and static approximations, respectively. Connections with a − sign are inhibitory, all the others are excitatory

original model in which the synapses converging to the on-off cell were modeled by static approximation, we used dynamic equations (indicated by the rectangle-shaped synapses). Our goal in this paper is not to capture in detail the spatial aspect of the receptive field, but rather to generate a simple connectivity pattern consistent with data generated by spatially localized stimuli. In order to keep the simulations simple, we consider only the horizontal extent of the receptive field. Furthermore, while the horizontal extent of the receptive field is reported to be approximately 7 cartridges (Jansonius and van Hateren 1993a), we simplify the network by allowing connections among only nearest neighbors.

3 Physiological interpretation of the model

Anatomically, L4 and L5 neurons do not receive any direct input from the photoreceptors (rev. Shaw 1984). Instead, they are fed by amacrine cells which are postsynaptic to the photoreceptors. Amacrine cells possess a dendritic organization that spans several cartridges. A direct interpretation of our neural network model suggests the following: The first-order cells represent photoreceptors, the second-order cells represent amacrine cells, and finally, the third-order cell represents the neurons anatomically labeled as L4 (see Shaw 1984).

This mapping along with our model for the sustained unit (Öğmen and Gagné 1990a) lead to the following predictions:

1. There must be at least two types of amacrine cells: on and off;
2. L4 and L5 units correspond to on-off and sustained units, respectively [this is contrary to earlier suggestions (see for example Laughlin 1984) but in agreement with the recent suggestion by Jansonius and van Hateren (1993b)];
3. On-amacrine cells make connections to sustained units (L5);
4. Both on- and off-amacrine cells make connections to on-off units (L4).

4 Simulations of the model

4.1 Methods

The model is described by a system of ordinary differential equations (ODEs) given in the Appendix. The system of ODEs was solved numerically using the adaptive step-size, Fehlberg, fourth-fifth-order, Runge-Kutta method. The FORTRAN code was obtained from Sandia Laboratories, Albuquerque, New Mexico via netlib electronic mail distribution (netlib@ornl.gov). The simulations were run on Sun Sparc workstations. The same set of parameters (given in Appendix) were used in all simulations.

4.2 Responses to luminance increments and decrements

Figure 3 shows the response of the model to luminance increments and decrements for a spatially wide-field (approximately 45 deg) stimulus. Here and in the following figures, the left column shows experimental data taken from Jansonius and van Hateren (1991) and the right column shows simulated model responses to the same stimulus. The traces under each panel indicate the temporal profile of the luminance of the stimulus. As can be seen from Fig. 3, the response has three components: One sluggish medium amplitude discharge locked to light increments, one brisk high amplitude response locked to light decrements, and finally, one weak discharge locked to light decrements. The model produces these three components and makes predictions about their origins: The sluggish on-response comes from the on-channel of the cartridge, the brisk off-response comes from the off-channel of the cartridge, and finally, the weak off-response comes from on-off cells of the neighboring cartridges via reciprocal connections between on-off units. A weak off-rebound similar to this third response-component was also observed in sustained-unit responses at the offset of a stimulus positioned in the inhibitory flank of the receptive field (Arnett 1972). We propose that the on-network of the on-off unit has a structure similar to the sustained network [see Öğmen and Gagné (1990a) for the model and simulations]. From the anatomical point of view, this suggests that the same putative on-amacrine population may subserve both the sustained and on-off units.

As shown in Fig. 3C, D and E, F, the response morphology is similar under light-adapted conditions. Despite some quantitative differences in the latencies and magnitudes of the response components, the model is in good qualitative agreement with data.

An aspect of the data which is not captured by the model is the high-frequency oscillations superimposed on the responses. Although the origin of these oscillations is not clear, the photoreceptor synapse has been suggested as a possibility (Jansonius and van Hateren 1991; van Hateren 1987). If this is the case, the corresponding equations need to be modified to capture these oscillations.

4.3 Temporal adaptation to on and off pulses

Jansonius and van Hateren (1991) studied extensively the temporal adaptation properties of the on-off unit by applying brief pulses of 10-ms duration with varying interpulse intervals. As shown in Fig. 4 A, C, E, and G, increasing the frequency of stimulation causes a strong adaptation in the amplitude of the responses. As one can see from model simulations (the right column), the model produces a qualitatively similar response.

Similar adaptation occurs for off-pulses as shown in Fig. 5. A comparison of Fig. 4C and Fig. 5C shows that adaptation to off-pulses occurs faster than adaptation to on-pulses. Overall, the model exhibits a similar behavior. Examination of Fig. 4G and Fig. 5G shows that for a

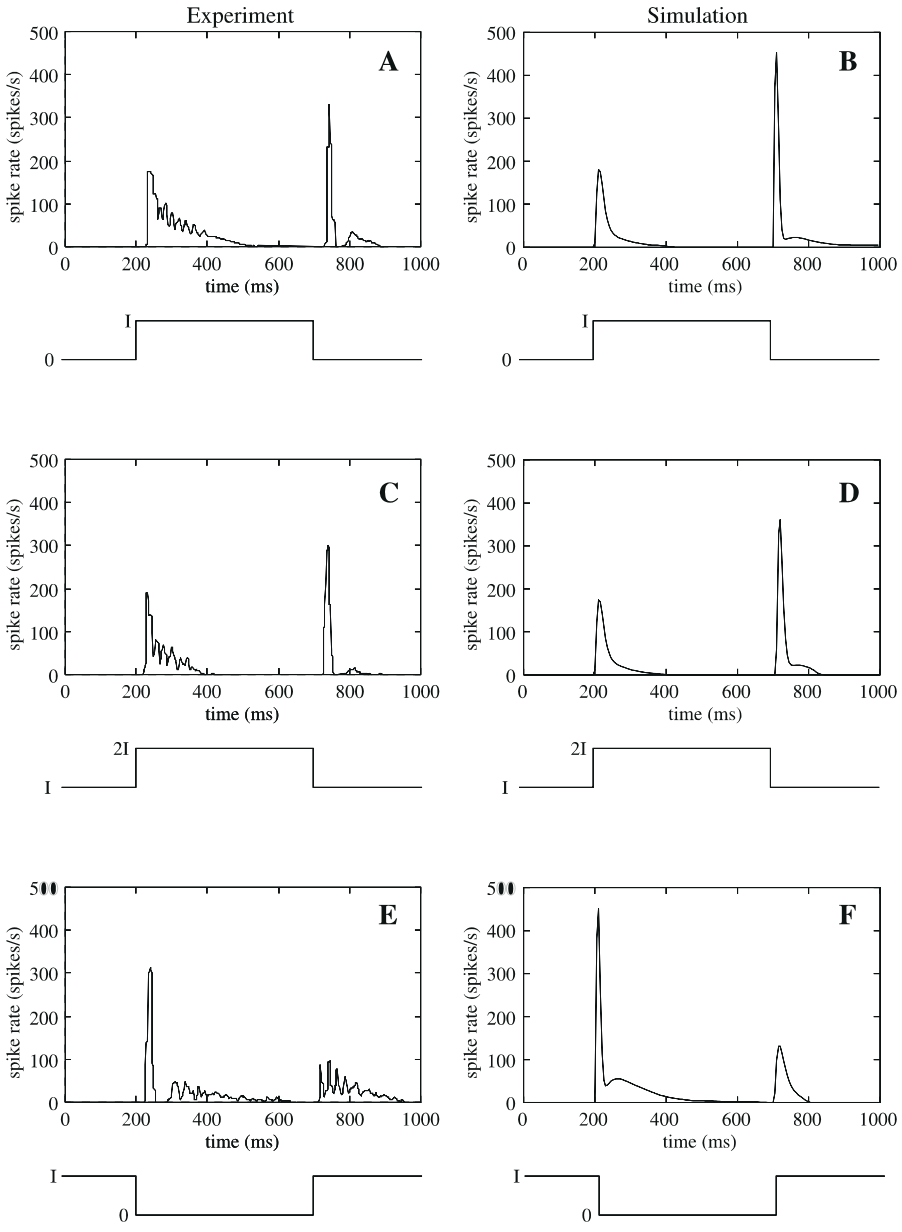

Fig. 3A–F. Responses of the on-off units to step inputs. The experimental data are from Jansonius and van Hateren (1991) and are shown in the *left column*. The responses of the model are given in the *right column*. **A,B** Response to 500-ms light pulse delivered during dark-adapted state. **C,D** Response to 500-ms light pulse delivered during light-adapted state. **E,F** Response to 500-ms luminance decrement applied during light-adapted state

maintained stimulus, the response amplitude tends to increase slightly. Furthermore, Jansonius and van Hateren reported the occurrence of an extra response-pulse when the stimulus frequency was high (see Fig. 5G). Although, similarly to the data, the model shows a small increase in the amplitudes of response-pulses,[2] no extra response-pulse is produced at the end of the stimulation. As discussed in the Appendix, with a different set of parameters it may be possible to obtain an extra pulse at the end of the stimulation. However, this did not occur with the parameters used in this study. In vivo, this feature seems also to be parameter dependent, for it has been reported to occur often but not always (Jansonius and van Hateren 1991).

The fast temporal adaptation occurs in the model at the synapses converging to the on-off cell. Since on- and off-channels converge via distinct paths, we propose that different adaptation time-constants emerge from different parameters of these pathways. This is also consistent with independent adaptation to on- and off-pulses (see Sect. 4.5).

4.4 Recovery

Figure 6 shows how the cell recovers rapidly when the frequency of stimulation is reduced. Initially, the cell is stimulated by on-pulses of frequency 20 Hz, and a rapid

[2] This increase is not visible in Figs. 4 and 5. The peak response values for on- and off-pulse responses were (281.983572, 123.600614, 80.073457, 67.921635, 64.532545, 64.430247, 64.417037, 64.770869, 65.165025, 65.496342, 65.742380) and (382.218567, 175.050357, 85.569583, 54.184584, 42.057448, 36.745579, 35.553368, 33.939205, 34.139199, 34.727553, 35.491839), respectively.

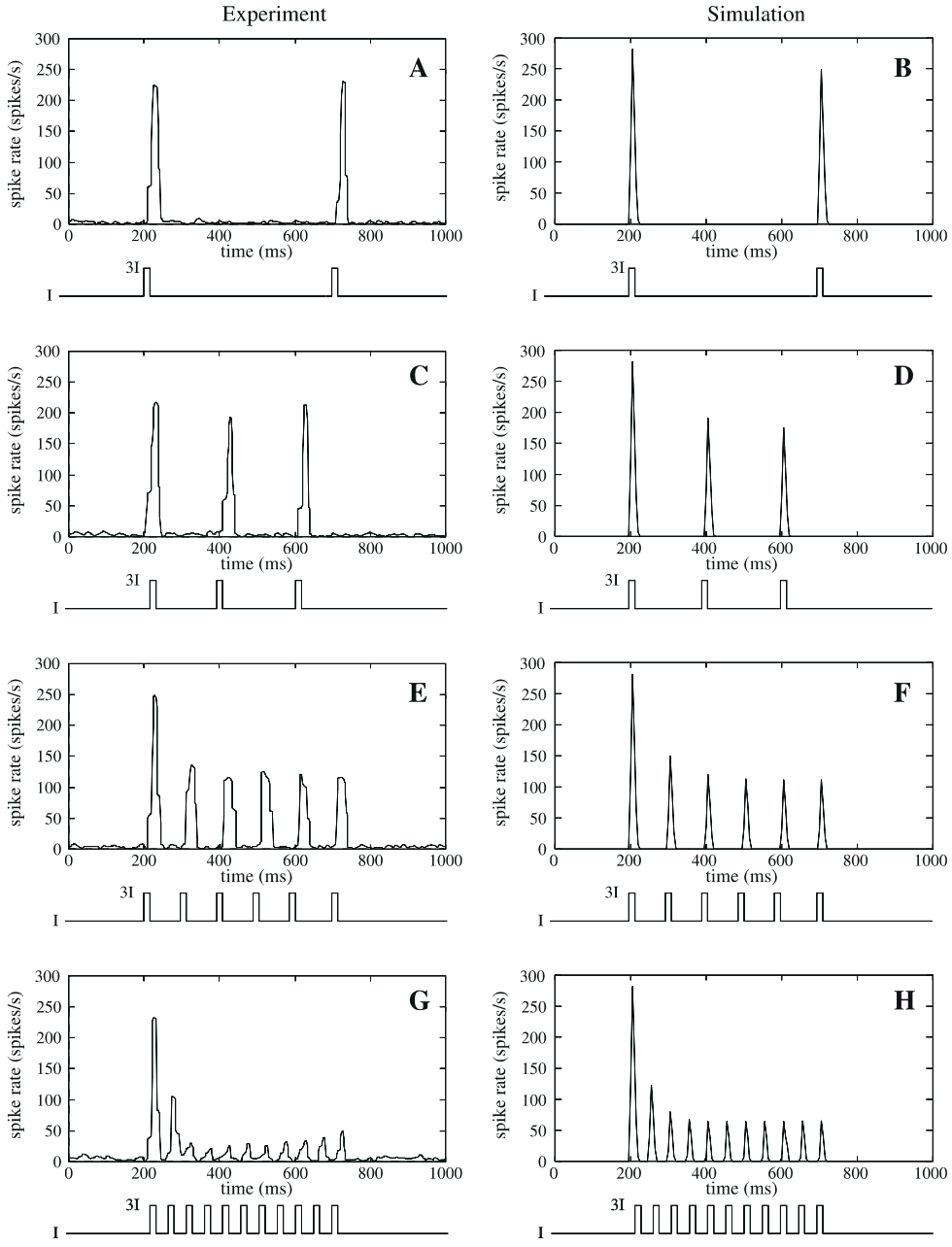

Fig. 4A–H. Responses of the on-off unit to a repetitive stimulation by 10-ms on-pulses during the light-adapted state. *Left column* shows the experimental data from Jansonius and van Hateren (1991). The model responses are shown in the *right column*. **A**,**B** Two pulses separated by 500 ms. **C**,**D** three pulses separated by 200-ms. **E**,**F** six pulses separated by 100 ms. **G**,**H** Eleven pulses separated by 50 ms

adaptation occurs. When the stimulation frequency is reduced to 10 Hz, the response magnitude increases from the first pulse onwards, both in the data and model.

4.5 Independence of adaptation to on- and off-pulses

In our model, the on- and off-pathways are segregated. Therefore, adaptation in these pathways prior to the convergence of on- and off-responses predicts that adaptation to on- and off-pulses will occur independently. Jansonius and van Hateren tested this hypothesis by using the experimental paradigm shown in Fig. 7.

First a control on (off) pulse was delivered. Following this control pulse, the cell was adapted by using off (on) pulses. Once adaptation had occurred, a test on (off) pulse was delivered. The responses to the test pulse show that adaptation to one pulse polarity does not cause adaptation to the other both in the data and in the model simulations. [3]

4.6 Responses to sinusoidal stimuli

In this simulation the input consisted of a sinusoidal-modulation of luminance in time with 100% Michelson

[3] Note that the experimental responses for the control conditions in this figure are weaker than the corresponding responses shown in Figs 4–6, causing a major quantitative difference between the model and the data. This is probably due to the variability of the physiological responses, unless a backward inhibition (cf. metacontrast) between the on- and off-systems is taking place.

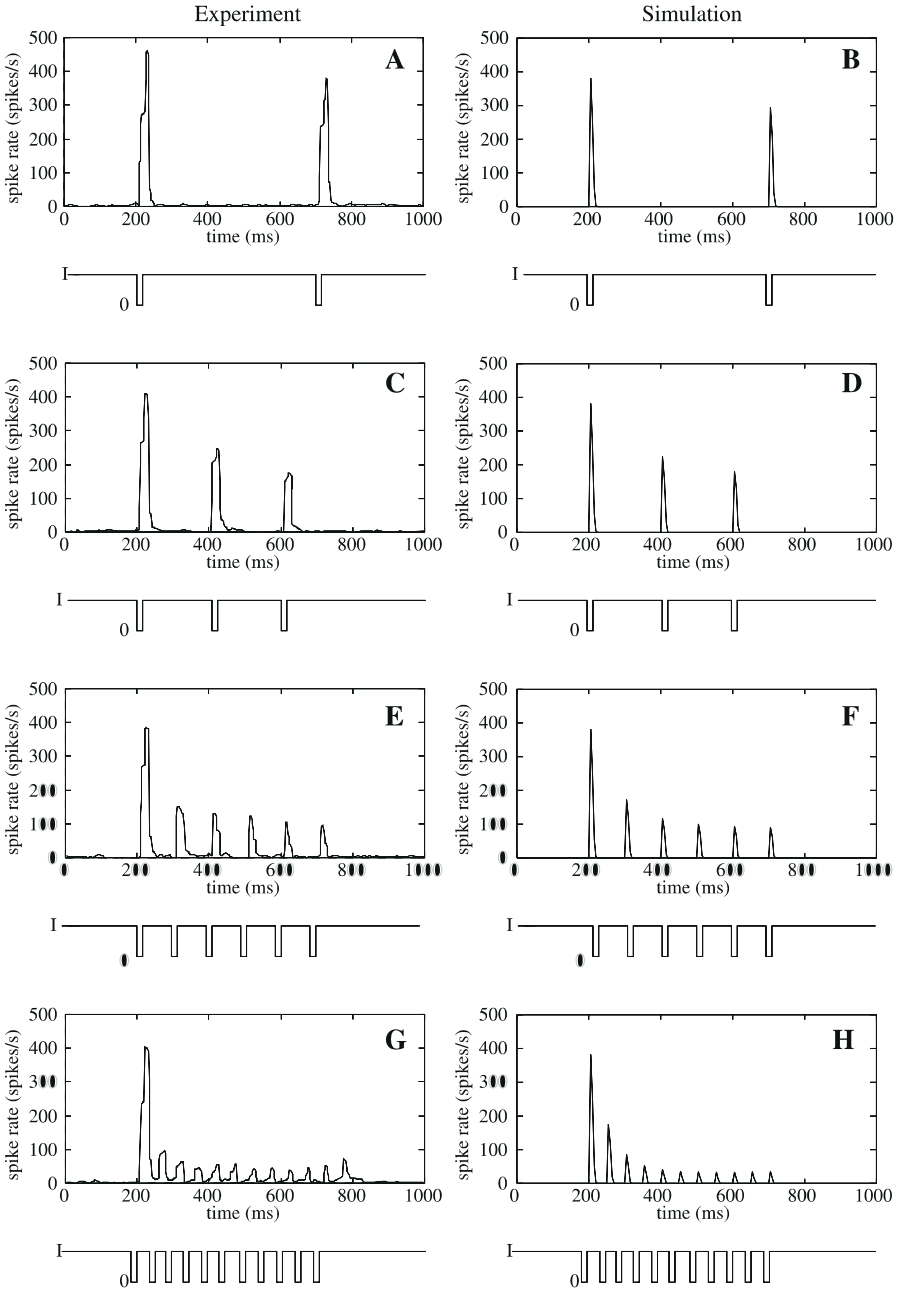

Fig. 5A–H. Same as Fig. 4 but for off-pulses

contrast. Figure 8A shows the response of the cell (spike rate averaged over 100 successive cycles) as a function of stimulus temporal-frequency and Fig. 8B, the results obtained from model simulations. Both frequency-response curves show band-pass characteristics. Quantitatively, in our simulations the peak of the temporal-modulation transfer-function occurs between 5 and 8 Hz. In the data, the peak occurs at 5 Hz. However, this is the only sample taken between 2 and 10 Hz. The model shows a broader frequency tuning than the data. Although the model gives a higher response at 20 Hz than the data, at 50 Hz the response vanishes in both the data and the model.

The phase characteristics, measured as the delay between the first peak (local maximum) of the cell response and the first peak of the stimulus divided by the period of the stimulus, are shown in Fig. 9A. For low temporal frequencies, the response leads the stimulus by approximately 90 deg analogous to the phase lead introduced by differentiation in a linear system (cf. transient nature of the system). At higher frequencies a phase lag is observed. The model (open diamonds in Fig. 9B) also shows a similar transition from phase-lead to phase-lag. Quantitatively, while both the model and data show similar phase characteristics at low temporal frequencies, the data exhibit a stronger phase lag than the model at high temporal frequencies. Figure 10 plots two of the sinusoidal responses (1 and 10 Hz) used to compute the frequency and phase characteristics shown in Figs. 8 and 9. These responses were obtained by averaging 1000 successive blocks, each with a duration equal to the period of the stimulus.

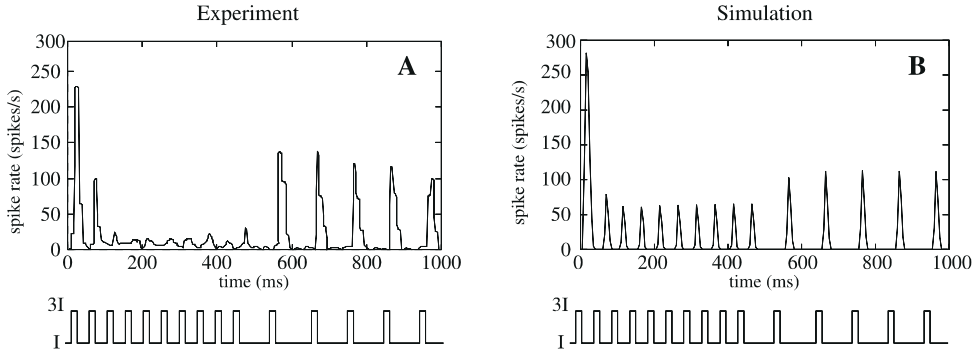

Figure 6A,B. Recovery from adaptation. Response to a train of pulses (10 ms duration) of frequency 20 Hz followed by a train of pulses of frequency 10 Hz. **A** The experimental data from Jansonius and van Hateren (1991). **B** The response of the model

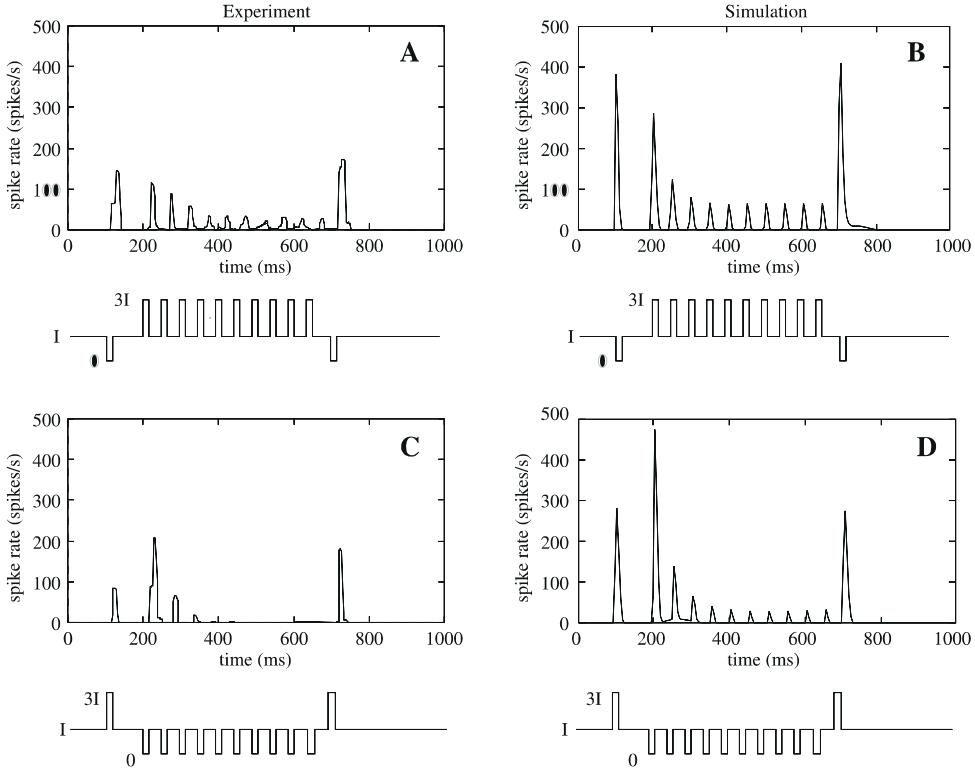

Fig. 7A–D Independent adaptation to on- and off-pulses. *Left column* shows the experimental data (Jansonius and van Hateren 1991). The responses of the model are given in the *right column*. A control pulse of a given contrast polarity is followed by a series of adapting pulses of opposite contrast polarity. After adaptation, a test pulse of the same contrast polarity as the control pulse is delivered. **A**,**B** Control and test pulses are of negative contrast polarity, while adapting pulses are of positive contrast polarity. **C**,**D** Control and test pulses are of positive contrast polarity, while adapting pulses are of negative contrast polarity

Model simulations (Fig. 10B, D) show a 'two-component response' corresponding to the 'on-' and 'off-phases' of the sinewave. The relative phase of these components shifts, as the frequency is increased from 1 to 10 Hz. Phase responses based on the time delay between the first local maximum of the response and the stimulus are shown in Fig. 9 by open diamonds and the model predicts phase values close to 90 and 0 deg for frequencies of 1 and 10 Hz, respectively. At 1 Hz, the data also show a two-component response. Note that both in the data and in the model one component starts at about $t = 0.5$ s, while the other component starts towards the end of the period and 'wraps around' to the beginning of the period. For 10 Hz, data show a noticeable but small component at about $t = 0.02$ s followed by a much stronger component around $t = 0.05$ s. The first component is similar in phase but weaker in amplitude when compared to the model-generated component at about $t = 0.025$ s. The phase response for the data in Fig. 9A seems to be computed from the second component; and this can explain why the phase in the data at 10 Hz exhibits a large lag when compared with the model-predicted phase based on the first local maximum. As mentioned above, in some cases a component 'wraps around' to the beginning of the period. The phase may also be defined using the maximum of the first component (instead of the first local maximum). If there is a wrap-around, the peak of the first component will correspond to the second local maxima in the response. For example, at $f = 10$ Hz, this criterion will use the peak at approximately $t = 0.075$ s to compute the phase (see Fig. 10D). The phase responses computed with this criterion are shown by the plus signs in Fig. 9. Normalized delays similar to those found in the data are observed. The data show that the two-component response observed at low frequencies is transformed into a single-component response as the frequency of stimulation is increased. As shown by the model response for

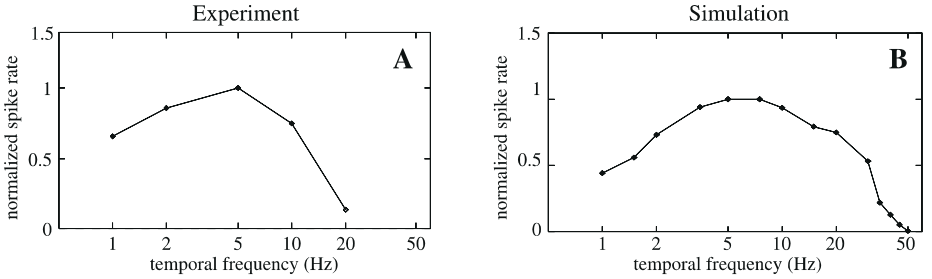

Fig. 8. Responses of the on-off unit to a sinusoidally modulated stimuli: **A** Normalized spike rate as a function of temporal frequency (experimental data from Jansonius and van Hateren 1991), **B** response of the model

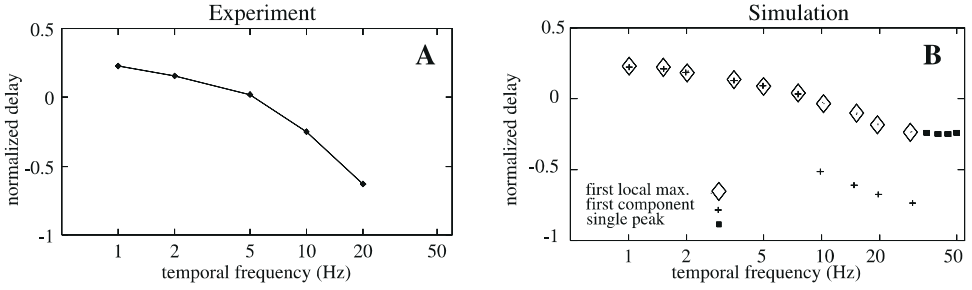

Fig. 9. Phase characteristics: **A** Normalized delay (normalized to the period of the sinusoidal stimulus) as a function of temporal frequency (experimental data from Jansonius and van Hateren 1991). **B** model predictions. Single-peak responses occur at high frequencies, and the phase values computed based on the delay of this peak are shown with *solid squares*. For lower frequencies, sinusoidal inputs generate double-peak responses, leading to two different criteria to compute phase (see text). Values resulting from the two criteria are shown by different symbols.

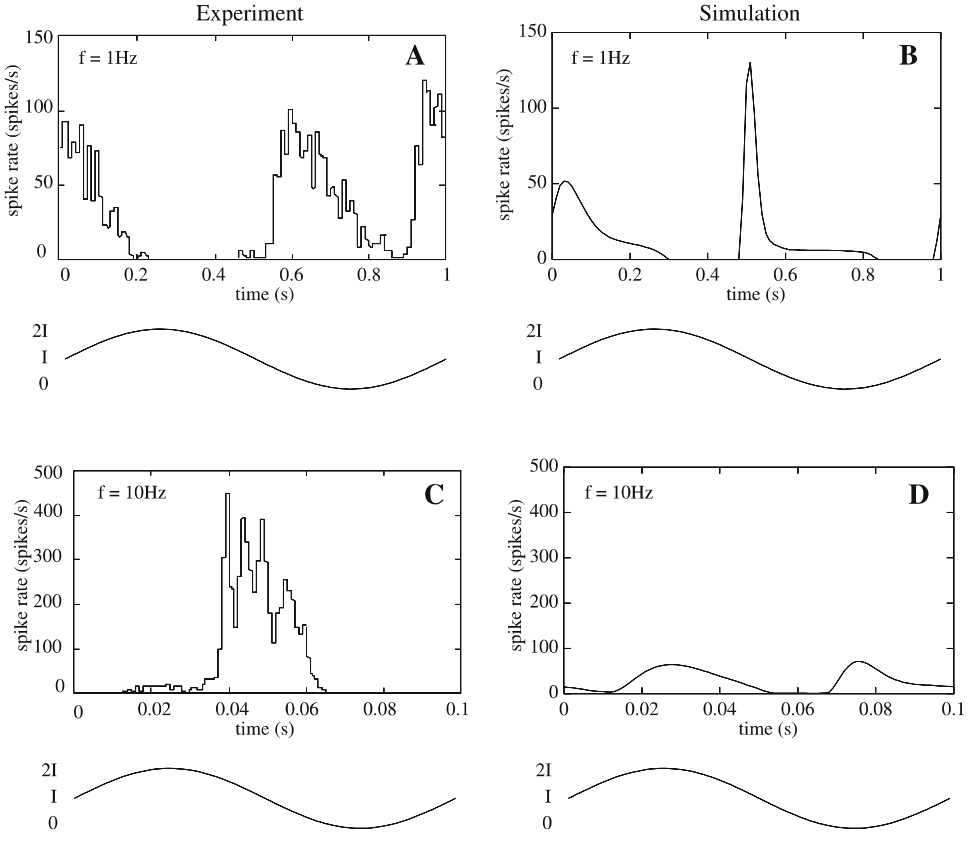

Fig. 10. Time course of responses to sinusoidally modulated stimuli of frequency 1 Hz (**A**,**B**) and 10 Hz (**C**,**D**). The *traces at the bottom of the panels* show the temporal profile of the stimuli. Experimental data, taken from Jansonius and van Hateren 1991, are shown on the *left*. model simulations on the *right*

$f = 40$ Hz (Fig. 11), a similar transformation occurs in the model but at higher frequencies. For frequencies with which a single component is observed, phase responses are plotted using solid squares.

Overall, while the model shows qualitatively similar sinusoidal responses, some quantitative differences are apparent. As mentioned earlier (see footnote 5), part of these quantitative differences could be due to the variability in the data.

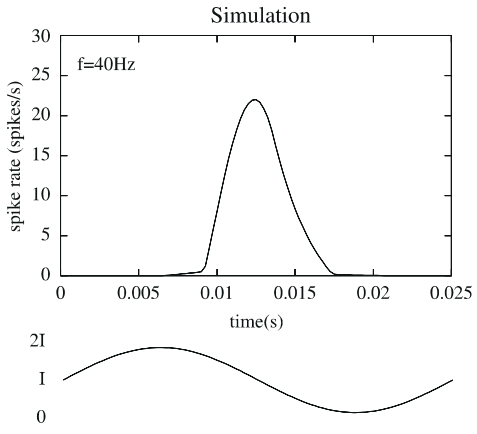

Fig. 11. Model-generated response to a sinusoidally modulated stimulus of frequency 40 Hz

4.7 Contrast sensitivity measured by step inputs

Figure 12 shows the average number of spikes elicited by the on-off unit in response to luminance steps of varying contrast levels. The unit is not very sensitive for contrast values of 10% and less. In our simulations, we found a higher contrast threshold. Although the electrophysiological findings and the model simulations differ from each other in terms of absolute contrast threshold values, this difference is mainly due to the simple linear-above-threshold function used in our simulations. Sigmoidal functions are better candidates but were not used in our simulations for reasons of simplicity.

5 Discussion

Notwithstanding some species-specific differences, spiking sustained and transient cells, similar to L4 and L5, have been found in several species. In the cat, for example, the X and Y retinal ganglion cells have sustained and transient responses, respectively (Enroth-Cugell and Robson 1966). In the primate visual system, neurophysiological data show a clear distinction between parvocellular (P) and magnocellular (M) populations in terms of the transience of their responses, at the level of both retina and LGN (Schiller and Malpeli 1977, 1978; Purpura et al. 1990). 'X-like' and 'Y-like' subpopulations of the M system have also been proposed (Purpura et al. 1990; Benardete et al. 1992). The presence of these cell types in the early visual system of several species suggests that they play an important role in some general visual function. One such function could be motion detection: The sustained and transient cells constitute the front-end of our motion detection model (Öğmen and Gagné 1990b; Öğmen 1997). In contrast, traditional models of motion detection have linear preprocessing [Reichardt 1961; van Santen and Sperling 1984, 1985; Adelson and Bergen 1985; Watson and Ahumada 1985). For most animals, the dynamic range of light intensity in their environment is much larger than the dynamic range of single neurons. Consequently, models with linear pre-processing face a saturation problem in vivo. Transient cells implement a temporal light adaptation by filtering the background light signal and thereby preventing a sustained saturation in postsynaptic cells. Several experimental findings in the fly visual system support the involvement of L4 and L5 in motion detection (McCann 1973; Riehle and Franceschini 1984; Coombe et al. 1989; Franceschini et al. 1989; Quenzer and Zanker 1991). The necessity for nonlinear pre- processing has also been demonstrated in the human visual system by use of stimuli that do not contain any directional information when filtered by a linear preprocessing stage (Chubb and Sperling 1988).

A second proposed functional role for the transient on-off neurons is the control of persistence in sustained neural cells subserving form perception (Breitmeyer and Ganz 1976; Öğmen 1993). In the human visual system, the percept generated by a static target outlasts the stimulus by a significant amount, a phenomenon known as visual persistence (e.g., Haber and Standing 1970; Coltheart 1980). The long duration of visual persistence suggests that objects should appear smeared when moving. However, under normal viewing conditions, moving objects appear sharp and clear, even if the moving object is blurred to some degree (Ramachandran et al. 1974; Bex et al. 1995; Hammett and Bex 1996). The reduction of perceived smear for moving objects is called motion deblurring (Burr 1980). Motion deblurring is proposed to result from the inhibition of sustained activities by transient on-off neurons (Di Lollo and Hogben 1987; Öğmen 1993; Chen et al. 1995). Similarly, the reduction in the perceived brightness of a target when preceded by a mask stimulus, as revealed in metacontrast masking experiments, is presumed to result from an

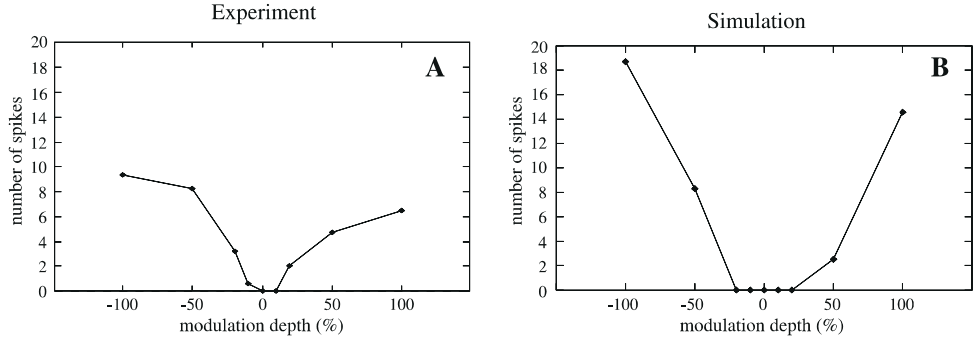

Fig. 12. Contrast sensitivity measured by step inputs: **A** Number of spikes elicited by different values of contrast (experimental data from Jansonius and van Hateren 1991), **B** model prediction

inhibition exerted by transient cells (Breitmeyer and Ganz 1976; Öğmen 1993).

The hypothesis that transient cells are involved in both motion detection and control of persistence in human vision is supported by experimental findings showing that apparent motion and metacontrast masking phenomena have similar properties (Kahneman 1967).

In summary, we presented an extension of our earlier model for transient cells in fly early vision. The extension introduced inhibitory interactions within the receptive field. This was achieved by lateral inhibition among on-cells in neighboring cartridges and a recurrent excitatory connection among the on-off cells. Furthermore, we also extended the use of dynamic synaptic equations from the early encoding to the level where signals from the putative on- and off-pathways converge to produce the on-off responses. Without dynamic synaptic equations at the first-stage of the model, the responses to step inputs will be sustained (cf. responses in Fig. 3). Without dynamic synaptic equations at the level of convergence, repetitive pulses will generate successive responses of the same amplitude (cf. responses in Figs. 4 and 5). The dynamic synaptic equations implement a form of short-term depression whose importance can be traced both at neural and behavioral levels.

At the neural level, synaptic depression helps adjust the gain of a synapse as a solution (in the temporal domain) to the 'noise-saturation dilemma' (Grossberg 1982). If a neuron receives a large number of synaptic inputs and yet has a limited dynamic range, then how can it detect reliably small signals (e.g., when only a few of the synapses are active) in the presence of noise, yet not saturate when the signals become large (e.g., when large number of synapses are active)? Synaptic depression allows the reduction of the gain of constantly active inputs (background), thereby making the postsynaptic cell more sensitive for changing, novel inputs. This suggests the use of synaptic equations with short-term depression for sites where the input signal varies considerably. At the input stage of the model, the luminance can vary significantly as the animal moves, for example, from a shaded region to a sunny region. At the level where connections converge from different parts of the receptive field, the signal arriving to the on-off cell can vary depending on how much of the receptive field is covered by the stimulus: A small moving object in front of an uniform background generates a small signal, while a moving textured background generates a large signal.

At the behavioral level, short-term synaptic depression can be viewed as a neural correlate for habituation, defined as a reduction in responsiveness to repetitive, predictable stimuli. When, for example, the animal is tracking a small object in front of a textured background, the signal generated by the small target will be buried under the large repetitive signal generated by the background. Habituation allows the filtering of the repetitive background signal, thereby enabling the processing of the target information. We have also shown elsewhere (Öğmen & Moussa 1993) how similar synaptic dynamics can account for the habituation observed in the landing behavior of the fly.

Acknowledgements: This study was supported by grant R29-MH49892 from NIH. We would like to thank Dr J.H. van Hateren for giving us permission to reproduce the experimental data.

Appendix: mathematical description of the model

Derivation of transmitter equations

If we denote by $s(t)$, $z(t)$, $y(t)$, and $x(t)$ the concentrations of S, Z, Y, and X, respectively, then the following differential equations can describe the dynamics of the biochemical system:

$$\begin{cases} \dfrac{dz}{dt} = -\gamma sz + \alpha x \\ \dfrac{dy}{dt} = \gamma sz - \delta y \\ \dfrac{dx}{dt} = \delta y - \alpha x \end{cases} \tag{6}$$

Since (2) [and equivalently (6)] is a closed system, we have $x(t) + y(t) + z(t) = \beta$, where β is a positive constant. Substituting this into (6), we obtain

$$\begin{cases} \dfrac{dz}{dt} = -\gamma sz + \alpha(\beta - y - z) \\ \dfrac{dy}{dt} = \gamma sz - \delta y \end{cases} \tag{7}$$

If we assume that the active state decays very fast (i.e. $\delta \gg \alpha, \gamma$), then the following approximation holds:

$$\begin{cases} \dfrac{dz}{dt} \approx -\gamma sz + \alpha\left(\beta - \dfrac{\gamma}{\delta} sz - z\right) \\ y(t) \approx (\gamma/\delta) s(t) z(t) \end{cases} \tag{8}$$

Rearranging the terms of the differential equation, one obtains:

$$\frac{dz}{dt} \approx -\left(\alpha + \gamma s[1 + \frac{\alpha}{\delta}]\right) z + \alpha\beta \tag{9}$$

Using $\delta \gg \alpha$, we get

$$\frac{dz(t)}{dt} \approx -(\alpha + \gamma s) z + \alpha\beta \tag{10}$$

Rearranging the terms yields

$$\frac{dz(t)}{dt} \approx \alpha(\beta - z) - \gamma sz \tag{11}$$

Model equations and parameters

The first stage is modeled by adaptation dynamics (possibly corresponding to adaptation in photoreceptors) following (11):

$$\frac{dz_{\mathrm{on},i}}{dt} = \alpha(\beta - z_{\mathrm{on},i}) - \gamma(I + J_i) z_{\mathrm{on},i} \tag{12}$$

and

$$\frac{dz_{\mathrm{off},i}}{dt} = \alpha(\beta - z_{\mathrm{off},i}) - \gamma I z_{\mathrm{off},i} \tag{13}$$

where indices on and off are introduced to designate the on- and off-pathways of the model (see Fig. 2) and index i refers to spatial positions. Both the on- and off-channels receive a common back-

ground signal I accounting for any residual activity in the dark-adapted state, but the external signal J_i is received by only the on-channel in the ith cartridge. The neural correlates for the parameters depend on the physiological interpretation of the equation. Accordingly, as mentioned in the text, a possible interpretation is to have $z(t)$ represent the amount of available transmitter, β the maximum amount of storable transmitter, α replenishment gain of transmitter, and γ depletion gain of transmitter, respectively. The parameter values were: $\alpha = 2.28$, $\beta = 4.29$, $\gamma = 0.35$, $I = 20$, and J was 0.0, 1.55, or 4.65 depending on the luminance of the input in the experiment.

At the second stage, on- and off-channels interact with inhibitory connections. Adapting (1) to the architecture of Fig. 2, one obtains:

$$\frac{dx_{\mathrm{on},i}}{dt} = -Ax_{\mathrm{on},i} + (B - x_{\mathrm{on},i})(I + J_i)z_{\mathrm{on},i} - (D + x_{\mathrm{on},i})v_1 \times \left[(I + J_{i-1})z_{\mathrm{on},i-1} + (I + J_{i+1})z_{\mathrm{on},i+1} + v_2 I z_{off,i}\right] \quad (14)$$

and

$$\frac{dx_{\mathrm{off},i}}{dx} = -Ax_{\mathrm{off},i} + (B - x_{\mathrm{off},i})Iz_{\mathrm{off},i} - (D + x_{\mathrm{off},i})v_1\left[(I + J_i)z_{\mathrm{on},i}\right] \quad (15)$$

where $x_{\mathrm{on},i}$ and $x_{\mathrm{off},i}$ denote the activities of the on- and off-cells in the ith cartridge, respectively. The term $(I + J_i)z_{\mathrm{on},i}$ represents the excitatory input and is substituted for the depolarizing conductance term (g^+) of (1). Similarly, the term $v_1[(I + J_{i-1})z_{\mathrm{on},i-1} + (I + J_{i+1})z_{\mathrm{on},i+1} + v_2 I z_{\mathrm{off},i}]$ is proportional to the sum of inhibitory inputs and is substituted for the hyperpolarizing conductance term (g^-) of (1). The equation for x_{off} results from the substitution of depolarizing and hyperpolarizing conductance terms with the excitatory and inhibitory inputs, respectively. For simplicity, V^{p} is assumed to be zero, and the constant A represents the passive conductance g^{p}. The parameter values were $A = 1.56$, $B = 285.36$, $D = 45.02$, $v_1 = 1.6$, and $v_2 = 0.25$.

At the third stage, the on- and off-signals from the same cartridge and on-off signals from the neighboring cartridges merge to give a combined on-off response. Synaptic dynamics at this level are described by

$$\frac{dw_{\mathrm{on},i}}{dt} = \alpha_{\mathrm{on}}(\beta_{\mathrm{on}} - w_{\mathrm{on},i}) - \gamma_{\mathrm{on}} G[x_{\mathrm{on},i} - \Gamma_{\mathrm{on}}]^+ w_{\mathrm{on},i} \quad (16)$$

and

$$\frac{dw_{\mathrm{off},i}}{dt} = \alpha_{\mathrm{off}}(\beta_{\mathrm{off}} - w_{\mathrm{off},i}) - \gamma_{\mathrm{off}} H[x_{\mathrm{off},i} - \Gamma_{\mathrm{off}}]^+ w_{\mathrm{off},i} \quad (17)$$

where $[.]^+$ is the 'linear-above-threshold' function (i.e., $[a]^+ = a$ if $a > 0$, $[a]^+ = 0$ otherwise), and the parameter values were: $\alpha_{\mathrm{on}} = 3.28$, $\beta_{\mathrm{on}} = 1.8$, $\gamma_{\mathrm{on}} = 1.5$, $\alpha_{\mathrm{off}} = 1.54$, $\beta_{\mathrm{off}} = 39$, $\gamma_{\mathrm{off}} = 24$, $G = 20$, $H = 6$, $\Gamma_{\mathrm{on}} = 27.6$, and $\Gamma_{\mathrm{off}} = 79.78$.

The on-off cell is characterized by

$$\frac{dy_i}{dt} = -A_y y_i + (B_y - y_i) \times \left(w_{\mathrm{on},i} G[x_{\mathrm{on},i} - \Gamma_{\mathrm{on}}]^+ + w_{\mathrm{off},i} H[x_{\mathrm{off},i} - \Gamma_{\mathrm{off}}]^+ + M[y_{\mathrm{del},i-1} - \Gamma_{\mathrm{on-off}}]^+ + N[y_{\mathrm{del},i+1} - \Gamma_{\mathrm{on-off}}]^+\right)$$

where $y_{\mathrm{del},i\pm1}$ is the feedback signal which is a low-pass version of the outputs of neighboring on-off units (modeling the dynamics of intracartridge lateral connections):

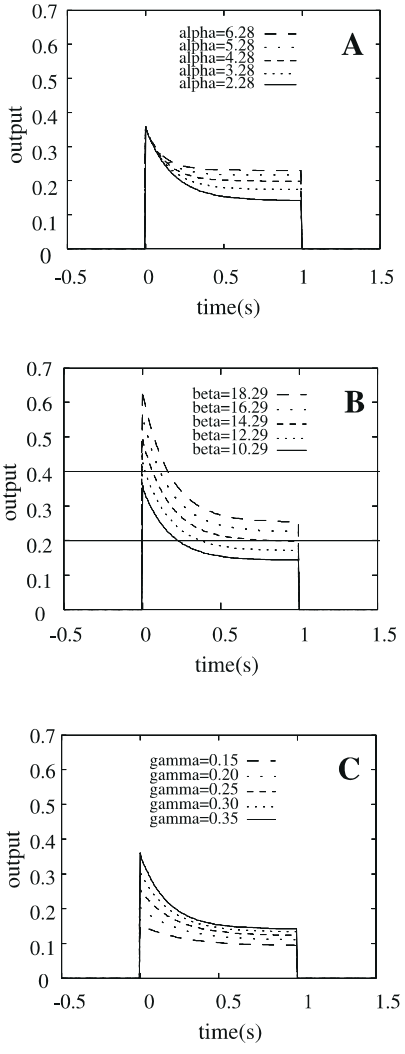

Fig. 13. Simulations illustrating effects of some parametric variations. All parameters, except the one shown in the *inset*, were kept fixed. Different plots show the responses generated by (21) for different values of the varying parameter. In **B**, *two horizontal lines* are drawn to help visualize the effect of thresholding the responses at 0.4 and 0.2

$$\frac{dy_{\mathrm{del},i\pm1}}{dt} = E\left(-A_{\mathrm{del}} y_{\mathrm{del},i\pm1} + (B - y_{\mathrm{del},i\pm1})F[y_{i\pm1} - \Gamma_{\mathrm{on-off}}]^+\right) \quad (18)$$

where E is a positive constant. The parameter values were $A_y = 351.12$, $B_y = 285.36$, $M = N = 0.1$, $E = 0.001$, $A_{\mathrm{del}} = 15800$, $F = 672$, and $\Gamma_{\mathrm{on-off}} = 3.5$.

The equation shown above implies that the on-off signal is a combination of the on- and off-signals in the stimulated cartridge and delayed on-off rebound signals from the adjacent cartridges. The relationship between the membrane potential of the third-order neuron and its spike frequency was chosen as a linear-above-threshold function $(6.0[y_i - 1]^+)$.

Effect of parameter variations

Since few data are available for the details of the circuit modeled in this paper, we were not able to incorporate physiologically estimated parameters into our simulations. Initial values of the parameters were chosen based on theoretical analysis (e.g., Öğmen

1997; sections 2 and 3) and our previous simulation studies (Öğmen and Gagné 1990a). These parameter values were then refined by trial and error to fit the experimental data.[4] Note that these parameter values are not unique, and other sets of parameters can produce similar behavior. To examine how the choice of parameter values affects the responses, let us note that the two fundamental differential equations used for membrane and transmitter dynamics can be written under the standard first-order time-varying differential equation form:

$$\frac{da(t)}{dt} = -A(t)a(t) + B(t) \tag{19}$$

where $A(t) = g^p + g^+(t) + g^-(t)$ and $B(t) = V^p g^p + V^+ g^+(t) + V^- g^-(t)$ for the membrane equation and $A(t) = \alpha + \gamma s(t)$ and $B(t) = \alpha\beta$ (constant) for the transmitter equation. The solution of (19) is

$$a(t) = \exp\left[-\int A(t)\,dt\right]\left(\int^t \exp\left[\int A(v)\,dv\right]B(v)\,dv + C\right) \tag{20}$$

where C is a constant. The specific form that this solution takes depends on $A(t)$ and $B(t)$ which, in general, depend on the external input. One can, however, gain insight into how parameter values influence the responses by considering the transmitter equation for a step input of amplitude u_0. Using (4) and (5), one obtains:

$$y(t) = \frac{\gamma}{\delta} u_0 \frac{\beta}{\alpha + \gamma u_0}(\alpha + \gamma u_0 e^{-(\alpha+\gamma u_0)t}) \tag{21}$$

One can see from this equation that steady-state (plateau) values are determined jointly by α, β, γ, δ, and u_0, while the transients, i.e., how fast the system reaches steady-state, is determined jointly by α, γ, and u_0. The initial overshoot at $t = 0^+$ is given by $y(0^+) = \frac{\gamma u_0 \beta}{\delta}$, which is independent of α. These points are illustrated numerically by the simulation results given in Fig. 13, where the different plots show $y(t)$ for various parameter choices.

The model is in general very sensitive to threshold parameters because of the nonlinearity it implies. To illustrate this, two different threshold values, 0.2 and 0.4, are shown in Fig. 13B by horizontal lines. Activities above the threshold line are transmitted, while those below it are not. For clarity, consider the response obtained with $\beta = 18.29$. One can see that changing the value of the threshold transforms the output from a brisk burst to a more sustained signal.

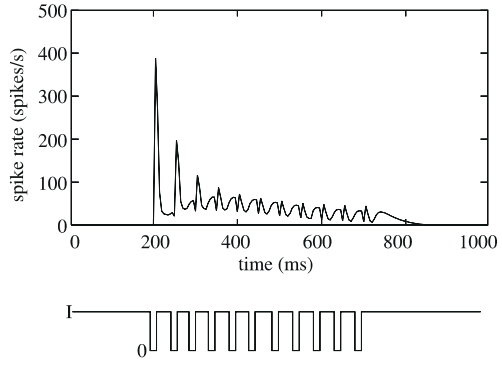

Fig. 14. Responses of the on-off unit to a repetitive off-pulse stimulation. In this simulation, the on-cell threshold Γ_{on} was lowered from 27.6 to 26.6

[4]Since our goal was not an exact quantitative fit, we found it easier to modify the parameter values "by hand" than by use of an optimization algorithm minimizing the error between the data and the model output.

Figure 14 shows a simulation where the threshold Γ_{on} of the on-cell was lowered from 27.6 to 26.6. A sustained response-component starts to 'leak' from the on-channel. An interesting result is the appearance of an extra-peak at the end of stimulation, similar to the one observed in the data of Fig. 5G. However, there does not seem to be a 'sustained leak' in the data. Whether a different set of parameters can remove the leak while keeping the extra peak remains an open question.

References

Adelson EH, Bergen JR (1985) Spatiotemporal energy models for the perception of motion. J Opt Soc Am A1:284–299

Arnett DW (1972) Spatial and temporal integration properties of units in the first optic ganglion of dipterans. J Neurophysiol 35:429–444

Benardete EA, Kaplan E, Knight BW (1992) Contrast gain control in the primate retina: P cells are not X-like some M cells are. Vis Neurosci 8:483–486

Bex PJ, Edgar GK, Smith AT (1995) Sharpening of drifting blurred images. Vision Res 35:2539–2546

Breitmeyer BG, Ganz L (1976) Implications of sustained and transient channels for theories of visual pattern masking, saccadic suppression, and information processing. Psychol Rev 83:1–36

Burr D (1980) Motion smear. Nature 284:164–165

Carpenter GA, Grossberg S (1981) Adaptation and transmitter gating in vertebrate photoreceptors. J Theor Neurobiol 1:1–42

Chen S, Bedell HE, Öğmen HA (1995) target in real motion appears blurred in the absence of other proximal moving targets. Vision Res 35:2315–2328

Chubb C, Sperling G (1988) Drift-balanced random stimuli: a general basis for studying non-Fourier motion perception. J Opt Soc Am 5:1986–2007

Coltheart M (1980) Iconic memory and visible persistence. Percept Psychophys 27:183–228

Coombe PE, Srinivasan MV, Guy RG (1989) Are the large monopolar cells of the insect lamina on the optomotor pathway. J Comp Physiol A 166:23–25

Di Lollo V, Hogben JH (1987) Suppresion of visible persistence as a function of spatial separation between inducing stimuli. Percept Psychophys 41:345–354

Egelhaaf A, Borst A (1992) Are there separate on and off channels in fly motion vision? Vis Neurosci 8:151–164

Enroth-Cugell C, Robson JG (1966) The contrast sensitivity of retinal ganglion cells of the cat. J Physiol 187:517–552

Franceschini N, Riehle A, LeNestour A (1989) Directionally selective motion detection by insect neurons. In: Stavenga DG, Hardie RC (eds) Facets of vision. Springer, Berlin Heidelberg New York, pp 360–390

Grossberg S (1972) A neural theory of punishment and avoidance. II. Quantitative theory. Math Biosci 15:253–285

Grossberg S (1982) Studies of mind and brain. D. Reidel, Boston

Grossberg S (1988) Neural networks and natural intelligence. MIT Press, Cambridge, Mass

Haber RN, Standing L (1970) Direct estimates of the apparent durtion of a flash. Can J Psychol 24:216–229

Hammett ST, Bex PJ (1996) Motion sharpening: evidence for the addition of high spatial frequencies to the effective neural image. Vision Res 36:2729–2733

Hateren van JH (1987) Neural superposition and oscillations in the eye of the blowfly. J Comp Physiol A 161:849–855

James AC, Osorio D (1996) Characterisation of columnar neurons and visual signal processing in the medulla of the locust optic lobe by system identification techniques. J Comp Physiol A 178:183–199

Jansonius NM, Hateren van JH (1991) Fast temporal adaptation of on-off units in the first optic chiasm of the blowfly. J Comp Physiol A 168:631–637

Jansonius NM, Hateren van JH (1993a) On-off units in the first optic chiasm of the blowfly. II. Spatial properties. J Comp Physiol A 172:467–471

Jansonius NM, Hateren van JH (1993b) On spiking units in the first optic chiasm of the blowfly. III. The sustaining unit. J Comp Physiol A 173:187–192

Kahneman D (1967) An onset-onset law for one case of apparent motion and metacontrast. Percept Psychophys 2:577–584

Laughlin S (1981) Neural principles in the peripheral visual systems of invertebrates. In: Handbook of sensory physiology, Vol. - VII/6B. Springer, Berlin Heidelberg New York, pp 133–180

Laughlin S (1984) The roles of parallel channels in early visual processing by the anthropod compound eye. In: Ali, MA (ed) Photoreception and vision in invertebrates. Plenum, New York, pp 457–481

Magleby KL (1987) Short-term changes in synaptic efficacy. In: Edelman GM, Gall WE, Cowan WM (eds) Synaptic function. Wiley-Interscience, New York, pp 21–56

McCann GD (1973) The fundamental mechanism of motion detection in the insect visual system. Kybernetik 12:64–73

Öğmen H (1993) A neural theory of retino-cortical dynamics. Neural networks 6:245–273

Öğmen H (1997) Sensorial non-associative learning and its implications for visual perception. In: Omidvar OM, Wilson CL (eds) Progress in neural networks, Vol. 5. Architecture. Ablex, New Jersey, pp 177–204

Öğmen H, Gagné S (1990a) Neural models for sustained and on-off units of insect lamina. Biol Cybern 63:51–60

Öğmen H, Gagné S (1990b) Neural network architectures for motion perception and elementary motion detection in the fly visual system. Neural Networks 3:487–505

Öğmen H, Moussa M (1993) A neural model for nonassociative learning in a prototypical sensory-motor scheme: the landing reaction in flies. Biol Cybern 68:351–361

Purpura K, Tranchina D, Kaplan E, Shapley RM (1990) Light adaptation in primate retina: analysis of changes in gain and dynamics of monkey retinal ganglion cells. Vis Neurosci 4:75–93

Quenzer T, Zanker JM (1991) Visual detection of paradoxical motion in flies. J Comp Physiol A 169:331–340

Ramachandran VS, Rao VM, Vidyasagar TR (1974) Sharpness constancy during movement perception. Perception 3:97–98

Reichardt W (1961) Autocorrelation a principle for evaluation of sensory information by the central nervous system. In: Rosenblith WA (ed) Principles of sensory communications. Wiley, New York, pp 303–317

Riehle A, Franceschini N (1984) Motion detection in flies: parametric control over on-off pathways. Exp Brain Res 54:390–394

Santen JPH van, Sperling G (1984) A temporal covariance model of human motion perception. J Opt Soc Am A1:451–473

Santen JPH van, Sperling G (1985) Elaborated reichardt detectors. J Opt Soc Am 2:300–321

Schiller PH, Malpeli JG (1977) Properties and tectal projections of monkey retinal ganglion cells. J Neurophysiol 40:428–445

Schiller PH, Malpeli JG (1978) Functional specificity of lateral geniculate nucleus laminae of the rhesus monkey. J Neurophysiol 41:788–797

Shaw SR (1981) Anatomy and physiology of identified non-spiking cells in the photoreceptor-lamina complex of compound eye of insects, especially diptera. In: Roberts A, Bush BMH (eds) Neurones without impulses. Cambridge University Press, Cambridge, UK, pp 61–116

Shaw SR (1984) Early visual processing in insects. J Exp Biol 112:225–251

Watson AB, Ahumada AJ (1985) Model of human visual-motion sensing. J Opt Soc Am 2:322–341